Analysis and Validation of Hydrokinetic Turbine Turbulent Wake Predictions

Sanchit Salunkhe[#,♣,1], Shanti Bhushan[#,♣,2], David Thompson[#,$,3], Timothy O'Doherty[*,4]

[#]*Center for Advanced Vehicular Systems*

[♣]*Department of Mechanical Engineering*

[$]*Department of Aerospace Engineering*
Mississippi State University, Starkville, MS 39759

[*]*School of Engineering*
Cardiff University, Cardiff, UK
[1]ss2976@msstate.edu; [2]bhushan@me.msstate.edu; [3]dst@ae.msstate.edu; [4]odoherty@cf.ac.uk

***Abstract*—** Turbulent simulations using URANS, DES and LES models are performed for a three-blade marine turbine appended with support struts. Predictions of thrust, power, and the mean and turbulent wakes in the near and intermediate wake region are compared with experimental data. The thrust and power coefficient predictions compare within 5% of the experimental data and results did not show significant dependence on turbulence modeling. The mean wake prediction compares within 7% of the data in the near wake, but shows large 25-35% errors in the intermediate wake. The large errors in the intermediate wake are due to poor predictions of cross plane turbulent fluctuations, which results in the under prediction of the wake diffusion and recovery. LES performs better than other models in the far-wake and behind the struts, when the resolved turbulence is triggered. However, shows the largest error in the intermediate wake as the turbulence in the blade tip region is not predicted accurately. Ongoing simulations are focused on understanding the role of numerical dissipation in the LES.

Keywords*— *Hydro-turbine, Wake, Computational Fluid Dynamics, Turbulence model, Validation

I. Introduction

Renewables such as wind and solar photovoltaic, whilst providing a valuable contribution to the energy mix, are unpredictable in the medium to long term and therefore cannot replace conventional fossil fueled power plants. The energy in the tides can be accurately predicted well in advance. This predictability is the main advantage of tidal energy [1]. While conventional, impounded hydropower is a well understood technology, hydrokinetic power generation can best be described as an immature technology that requires additional research and development [2]

Research on the wind/hydro turbines are essentially divided into two principal domains: the prediction of rotor performance [3] and the study of the wake [4]. Wake dynamics are extremely important when arrays of these devices are considered. Experimental and computational studies have helped in understanding the characteristics of the wake behind wind/hydro turbines [5]. The flow behind a wind turbine is sub-divided in three regions.

(a) Near wake region: It extends up to 1*D* downstream, where *D* is the turbine diameter, and the flow in this region is dominated by the velocity deficit due to the energy extraction and the vortices created at the tip of the rotor blades. The flow structure in this region essentially depends on the aerodynamic characteristics of the rotor blades.

(b) Intermediate wake region: It extends up to 4-5D, wherein the tip vortices gradually lose identity, and the undisturbed flow mixes with the core flow. As a result, the wind speed deficit and the turbulence generated from the blade begin to decay. The shear layer developing from the blade tips moves towards the centreline. As the shear layer reaches the wake axis, it marks the beginning of the far-wake region [6].

(c) Far wake region: It extends beyond 5D and the wake profile in this region is typically assumed Gaussian. The flow in this region is dominated by the convective and turbulent diffusion, where the latter is due to both the turbine generated shear layer and ambient turbulence. The turbulence feeds energy into the mean flow causing decay in both the wake deficit and turbulence [7].

Some studies have also reported wake meandering in the far wake region, wherein wake moves both in the horizontal and vertical directions even for constant upstream mean flow, and smears the velocity deficit and the extra turbulence over a much larger volume than that for a fixed wake [8].

The near wake research primarily focuses on the performance and the physical process of power extraction, and rely on blade element momentum methods (BEM) who's accuracy depends on the availability of the airfoil data [4,9]. The focus of far wake research is on the prediction of wake deficits to evaluate the mutual influence when the turbines are placed in clusters, and their effect on power production. The far-wake computational studies assume that the modelling of the rotor is less critical in this region, and computations focus primarily on wake evolution models [10-12] as well as on wake interference and turbulence models [13,14]. Such models strongly rely on the initial velocity and turbulent kinetic energy profiles generated by similarity profiles. Vermeer et al. [5] noted that the flow physics in the intermediate wake region are not very well understood, and is an area of active research.

Computational Fluid Dynamics (CFD) approach, using solutions of the Navier-Stoke equations provide an option to predict both the near-, intermediate- and far-wake regions,

without additional turbine blade modeling. One of the primary challenges for such simulations is the modelling of the rotating turbine blade. Various modelling strategies have appeared in the literature for this purpose, which can be categorized either as actuator or discretized rotor models [15].

In actuator models, body force terms are added to the Navier-Stokes equations to mimic the fluid momentum extracted by the rotating turbine blades, whereas in the discretized rotor model the turbine blades are explicitly resolved. The actuator models are computationally inexpensive compared to the discretized rotor model as they save mesh points because the blade boundary layer does not need to be resolved, and enable representation of rotating blades without having to use moving meshes. The actuator disk model is the most commonly used in wind/tidal turbine simulations [16,17]. The model has been improved over the years to better capture the three-dimensionality, swirl [18] and turbine induced turbulence [19] in the flow. The primary limitations of this approach are that it fails to capture the tip vortices generated from the turbine, and it does not account for the transient flow characteristics.

The actuator line model extends the disk model, wherein the body force is applied (or aerodynamic loading is distributed) along a line that represents the current position of a blade, and the lines rotate following the motion of the blade [20,21]. This method provides a reasonably physical representation of the wind turbine blade compared to the disk model, and captures the tip vortices reasonably well. Shen et al. [15] noted that actuator line models capture the turbine surface only as a point, so it is not expected to capture the details of flow past a surface. The study introduced a 2D actuator surface model, wherein the body force (or aerodynamic loading) is distributed over a surface.

Full-turbine models are computationally expensive because of the widely-disparate spatial scales that must be resolved [22]. For full rotor models using body-fitted grids, simulations can be divided predominately into three types: (1) the single frame model; (2) the rotating frame model and (3) the rotating blade model.

In the single reference frame model, the computational domain rotates with the turbine [4]. The unsteady flow produced by the turbine becomes a steady flow relative to the rotating frame, which simplifies the simulation. Unfortunately, it is not possible to simulate a support or the free surface in the single-frame model.

In the rotating frame model, the flow in the domain encompassing the rotating turbine and rotor gemetries is solved in a rotating reference frame, whereas the flow elsewhere is solved in Earth fixed coordinate frame. The two domains communicate via an interface boundary [23,24]. Such simulations capture the near-wake well, but predicts frozen tip vortices and wake. Such simulations are inexpensive compared to the rotating blade model, as grid rotation is not involved and provides a reasonable mean wake prediction.

In the rotating blade model, the domain encompassing the rotating turbine and rotor geometries rotates physically, and communicates with the outer domain via either a sliding interface or an overset mesh [25-27]. This method is numerically the most expensive, but provides the most accurate blade modeling.

One of the challenging issues for the prediction of the turbine wake is the turbulence, and most simulations have been performed mostly using Reynolds avereged Navier-Stokes (RANS) [4,17], and limited studies have used detached eddy simulation (DES) [22]. Kasmi et al [28] reported that the standard k-ε RANS model overpredicts turbulence kinetic energy (TKE) in the regions of high mean shear, i.e., in the near/intermediate wake behind the tip blade thereby increasing the turbulent diffusion and underpredicting velocity deficit. The study proposed a modification to the model, wherein a turbulence dissipation term is addded to limit the turbulent kinetic energy (and viscosity) in the region mentioned above. Shives and Crawford [29] proposed a similar model, and validated it for hydro-turbine predictions. Cabezon et al. [30] compared various linear and anisotropic RANS models, and concluded that Kasmi et al. approach greatly improves wake deficit predictions compared to the standard k-ε model. They also reported that the anisotropic models perform similar to the isotropic models. They further noted that all models tend to underestimate the near wake turbulence intensity and perform best along the axis. Elvira et al. [6] emphasized that the near and intermediate wake recovery are dominated by the turbulence anisotropy. They performed simulations using an anisotropic turbulence model for wind turbine wake prediction and reported good agreement with experimental data. However, the study concluded that the tip vortices and associated shear-layer, that involve large-scale coherent structures, cannot be captured well in RANS; thus, the best option is to perform large eddy simulation (LES). Note that all of the above studies have used actuator disk models, thus the turbulence modeling limitations may not be applicable for full-turbine models.

The objective of this study is to validate hydro-turbine (intermediate $1.5D - 7D$) wake predictions using a rotating blade model against recently procured flume experimental data [1], including a study of the effects of turbulence modelling, grid resolution, and support structure on the wake predictions, and analysis of vortical and turbulent structures to understand the wake development mechanism. For this purpose, Ansys/Fluent simulations are performed using RANS, DES, and LES models using both manually refined and solution adapted grids consisting up to 8.8M cells. The validation focuses on the prediction of the integral quantities (thrust co-efficient and power co-efficient), wake recovery, velocity components in the wake, turbulent kinetic energy in the wake, and the mean and turbulent characteristics of the intermediate and far-wake regions.

II. Experimental Data

Experiments were performed in a recirculating flume in the University of Liverpool to investigate the near-wake characteristics of a three-bladed, horizontal axis hydro-turbine [1]. The turbine used in the study has Wortmann FX 63-137

blade profile with 6° pitch angle and D = 0.5m. The blades were connected to hub by means of connector pins as shown in Fig. 1 [31]. The experiments were performed in a water depth of 0.8m. The turbine was supported from above using a cylindrical strut such that the turbine axis was kept at 0.425 m depth. Thus the tip of the turbine was 0.175m (or 0.7D) below the free-surface, and 0.125m (or 0.5D) above the bottom wall. The test section has a spanwise extent of 1.35 m, thus the blade tip clearance along the spanwise direction was 0.425 m (or 0.85D). The support strut was located 0.6D behind the blades.

Experiments were performed for a specified tip speed ratio,

$$\lambda = \frac{\omega D}{2U_0} = 3.65 \quad (1)$$

where, ω ~~= 21.92 rad/s~~ is the blade rotation speed~~,~~ and U_0 is the inflow velocity. U_0 ~~The inflow velocity~~ was reported to be in the range ~~U_0 =~~0.5 – 1.5 m/s with turbulence intensity of 2%, the blade rotational speed was ~~and~~in ~~–~~the range 7.3 – 21.9 rad/s the Reynolds number of the flow based on inflow velocity and turbine radius ranged between ~~was~~ ~~*Re* =~~ 2.22×10^5 ~~-~~ 6.66 x 10^5. Above 1 m/s the performance characteristics are independent of Re [31xx].

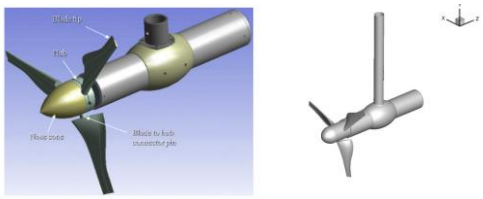

(a) (b)

Fig. 1 (a) Photograph of the turbine blade and support assembly (taken from [1]), and (b) turbine blade and support structure model in CFD simulations.

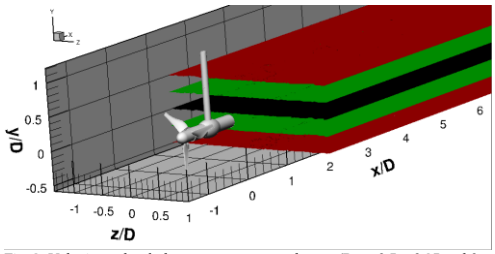

Fig. 2 Velocity and turbulence measurement planes y/D = ±0.5, ±0.25 and 0.

The experimental data included: thrust (C_T) and power coefficients (C_P); contours of streamwise (x), transverse (y) and spanwise (z) velocities for streamwise locations x/D = 1.5 to 7 at five transverse planes (along water depths) y/D = ±0.5, ±0.25 and 0 (shown in Fig. 2); maximum wake deficit at x/D = 1.5 to 7 at y/D = ±0.5, ±0.25 and 0 planes; Streamwise turbulent velocity fluctuation u' and TKE profiles with respect to z/D at x/D = 1.5 to 7 at y/D = 0; maximum Reynolds normal and shear stresses and TKE at x/D = 1.5 to 7 at y/D = ±0.5, ±0.25 and 0 planes; and turbulence anisotropy map in the wake. The experimental uncertainty was reported to be 1%.

III. Tidal Stream Turbine Computational Model

The simulations were performed using the commercial flow solver ANSYS/Fluent® version 14.0 [32]. The flow fields are governed by incompressible Navier-Stokes equations in moving reference frame. Turbulence models assume decomposition of the instantaneous velocity (u_i) into resolved ($\hat{u}_i$) and modelled (u'_i) components:

$$u_i = \hat{u}_i + u'_i \quad (1)$$

where, velocities are defined in the Earth-fixed reference frame, and i are the three directions. The $(\cdot)$ represents Ensemble averaging for RANS, and grid filtering for DES and LES. Application of the averaging/filtering operation to the Navier-Stokes equations yields,

$$\frac{\partial \hat{u}_i^r}{\partial x_i} = 0 \quad (2)$$

$$\frac{\partial \hat{u}_i}{\partial t} + (\hat{u}_j^r \frac{\partial \hat{u}_i}{\partial x_j}) + \tilde{\omega} \times u = -\frac{1}{\rho}\frac{\partial \hat{p}}{\partial x_i} + \upsilon \frac{\partial^2 \hat{u}}{\partial x_j \partial x_j} - \frac{\partial \tau_{ij}}{\partial x_j} \quad (3)$$

where, $\hat{u}_i^r = \hat{u}_i - \tilde{\omega} \times R$ is the relative velocity, $\tilde{\omega} = (0,0,\omega)$ is the turbine rotation vector, and ***R*** is the radial location vector. The τ_{ij} term on the right-hand side represents the turbulent stresses, which are modeled based on Boussinesq assumption :

$$\tau_{ij} = -\nu_T S_{ij} \quad (4)$$

where, ν_T is the turbulent eddy viscosity and S_{ij} is the rate-of-strain tensor. The different turbulence models vary in the definition of the turbulent eddy viscosity, as discussed below.

A. Turbulence Modelling

Turbulent simulations are performed using unsteady RANS (URANS) and high fidelity DES and LES models, since the wake is expected to be turbulent. URANS simulations are performed using the *k-ω* shear stress transport (SST) [33], and Spalart-Allmaras (SA) [34] models. Hybrid RANS/LES (HRL) were performed using both SA- and SST-based improved delayed DES (IDDES) models [35]. LES were performed using the monotonically integrated LES (MILES) approach [36]. Readers are referred to the cited reference for the details of the models. The following summarizes the key points of the IDDES and MILES models.

The IDDES model modifies the modeled dissipation term based on the computed largest energy containing turbulent length-scale (l) and the grid scale (Δ), such that the dissipation is same as that of URANS for large grid sizes ($\Delta \geq F_{HRL}\times l$), where F_{HRL} is a model coefficient. However, for smaller grid sizes, the modeled dissipation is reduced to enable resolved TKE predictions. MILES does not include any turbulence modelling and it is assumed that the numerical dissipation is of the same order of magnitude as that of subgrid stresses in the LES. Previous studies have shown that, in Fluent simulation for free-shear flows, the MILES models perform better than LES models [36] using 2^{nd} order schemes.

Formatted: Superscript

However, for wall bounded flows, they are not expected to be accurate for the prediction of the boundary layer.

B. Numerical Methods and High Performance Computing

Fluent is a message passing interface (MPI) based finite volume solver providing a suite of numerical schemes. Transient simulations were performed using the pressure-based solver option, which is the typical predictor-corrector method with the pressure update based on a Poisson equation designed to produce mass conservation. Pressure-velocity coupling was performed using the Pressure-Implicit with Splitting of Operators (PISO) scheme. Unsteady terms were discretized using a 2nd-order implicit (three-point backward difference) scheme. The convective terms in the momentum equations were discretized using a 2nd-order upwind scheme for URANS and Bounded Central Difference (BCD) for DES, IDDES, and MILES. The BCD scheme seeks to include just the right amount of dissipation to balance the sum of the aliasing and finite-differencing errors, and is recommended for hybrid RANS/LES simulations using FLUENT [36].

Simulations were run on 48 processors for about 80K time steps, which corresponds to 160 turbine blade rotations, and each timestep took 40s of CPU time. The total CPU run time was about 37days and 43K CPU-hours.

IV. Grids, Simulation and Boundary Conditions

Simulations were performed in a domain of dimensions 26D×2.7D×1.9D along *x*, *z* and *y* directions, respectively. The simulation domain is shown in Fig. 3. The spanwise extent of the domain is same as that of the experimental test section, and the transverse domain corresponds to the water depth in the experiment. The *x* domain extends from -5D upstream (inlet) to 21D downstream (outlet) based on previous study [37] such that the simulation is not affect by the inlet and outlet boundaries .

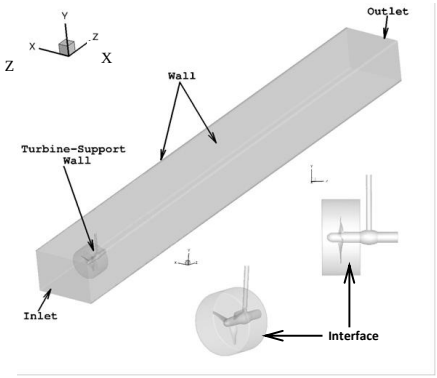

Fig. 3 Simulation domain and boundary conditions. Inset figure shows the rotating cylindrical domain for turbine blades and hub.

The simulation also includes an embedded cylindrical domain for the turbine blade and hub (Fig. 3), which rotates with the turbine angular velocity. The cylinder domain provides an interface between the moving mesh and stationary mesh, which communicates flow information between the rotating and static domains. Three hybrid hexahedral-tetrahedral cell grids, consisting of 3M (coarse), 5.5M (medium), and 8.8M (fine) cells, were generated for the study. The hexahedral cells were used in the boundary layer and tetrahedral cells elsewhere. Representative plots showing the grid resolution and refinement is presented in Figure 4. The medium grid included grid refinement in the near and intermediate wake regions, x/D = 0.4 - 7; and both y/D, z/D = -0.6 - 0.6. The fine grid included solution based grid adaptation in the tip vortex region. The skewness of the grids varied from 0.01 to 0.98. The cell aspect ratio varied from 0.5 to 318, with an average value of ~10. The maximum aspect ratio was obtained in the boundary layer, as expected. The high aspect ratio cells were obtained close to the blade tips at the intersection of hexahedral and tetrahedral cells.

Wall boundary condition are used along both the spanwise and transverse faces. Note that the y_{max} face is the free surface (air-water interface) in the experiments, thus the simulations do not include the free-surface effect. The near wall grid resolution showed averaged y^+~17 on the turbine blades, with maximum value y^+~42 towards the blade tips. The cell wall distance was large y^+~300 for the spanwise and transverse direction walls. Thus, wall-functions were used for the viscous wall boundary condition. A zero pressure boundary condition is used at the outlet.

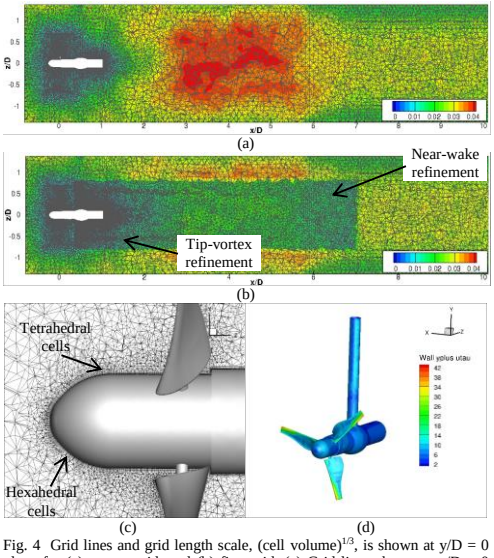

Fig. 4 Grid lines and grid length scale, (cell volume)$^{1/3}$, is shown at y/D = 0 plane for (a) coarse grid, and (b) fine grid. (c) Grid lines shown at z/D = 0 plane close to the hub to show the usage of mixed hexahedral-tetrahedral cells. (d) y^+ distribution on the turbine blades.

Simulation conditions included a uniform streamwise inlet velocity (U_0) = 0.892 m/s and a turbulence intensity of

2%, following the experiments, which resulted in *Re* = 2.2×10^5 based on ν of water at T = 20°C. The turbine grid block rotated at 21.9 rad/s. The simulations performed in the study are summarized in Table 1. The study consisted with 10 simulations using 3 grids, 5 different turbulence models including a study to evaluate the effect of inlet turbulence viscosity specification on the predictions (by comparing cases 6 and 7). Most of the discussion in the paper focuses on the medium grid solutions in cases 6, 8 and 9. The case 10 solution on the fine grid is still being processed.

V. Results

A. Thrust and Power Predictions

The thrust and power predictions were unsteady for all of the models and grids. In both URANS and IDDES, the unsteadiness was primarily large scale with a 1% variation around the mean with a dominant frequency f = 10 Hz, as shown in Fig. 5. LES predicted an 8% variation in the C_P, significantly larger than URANS/IDDES, and also shows a dominant peak f ~ 10 Hz, and a second peak at f ~ 16 Hz. Note that the dominant frequency of 10Hz corresponds to $N\times\omega/2\pi$, where N is number of blades. The dominant frequency identified above has been well documented in the literature due to the tower-shadow effect [38]. The tower-shadow effect is due to disruption of the flow each time a blade passes the tower. This results in power fluctuations frequency equal to number of blades times the turbine rotational frequency. The second peak in MILES is expected due to resolved turbulence unsteadiness.

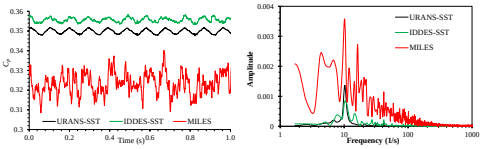

(a) (b)

Fig. 5 (a) Time history and (b) FFT of URANS, IDDES and MILES C_p predictions obtained using the medium grid.

Table 1 Summary of simulations, including grids and turbulence models, used in the study and prediction errors for C_T, C_P and wake.

Case	Grid	Turbulence Model		Thrust C_T	Thrust $\%C_{T,p}$	Thrust $\%E_T$	Power C_P	Power $\%E_p$	$\%E_{wake}$
Experiment				*1.0*	-	-	*0.34*	-	-
1	3M	URANS	SST	1.041	99.18	4.1	0.351	3.2	21.44
2			SA	1.046	98.75	4.6	0.353	3.8	21.49
3		DES	SST	1.034	98.66	3.4	0.358	5.3	21.32
4			SA	1.034	99.08	3.4	0.359	5.6	22.07
5		LES	MILES	1.048	99.24	4.8	0.322	-5.3	22.55
6	5.5M	URANS	SST	1.042	98.7	4.2	0.348	2.4	24.1
7			SST, ν_T/ν =1	1.041	98.5	4.1	0.348	2.4	24.1
8		DES	SST	1.036	98.68	3.6	0.357	5.0	23.8
9		LES	MILES	1.053	99.22	5.3	0.325	-4.4	25.7
10	8.8 M	LES	MILES	1.052	99.23	5.2	0.323	-5.0	-

Both C_T and C_P were primarily (about 98-99%) due to the wall pressure distribution as shown in Table 1. All of the simulations agree within 5% of the data for C_T and C_p. The simulations over predicted C_T, but show mixed over and under predictions for C_P. In particular, URANS/IDDES are over predictive and MILES is under predictive.

B. Overall Flow Predictions

As shown in Fig. 6, all of the simulations show vortex generation from the blade tips, which spirals forming vortex rings, and are advected downstream. The vortex rings are eventually destroyed due to the impact with the support structure. As reported by [37], without the support structure, the tip vortex rings are advected far downstream. This suggests that the support structure significantly affects the wake. The flow also shows significant vortex generation from the support structure. The structure of the tip vortex rings and the vortices from support structure are resolved better in MILES followed by IDDES and then URANS.

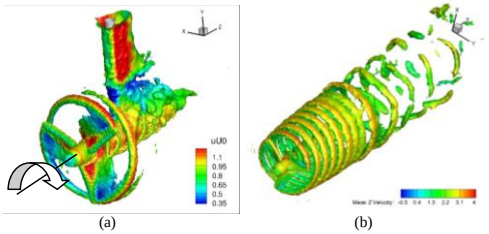

(a) (b)

Fig. 6 Vortical structures predicted using MILES for simulations (a) with support structure, and (b) without support structure [37].

The flow around turbine blade is analyzed at: y/D = -0.25 (close to the root) and -0.4 (close to the tip) to investigate flow separation and tip vortex generation, as shown in Fig. 7. The windward surface pressure distribution in Fig. 7(a) shows low pressure towards the blade leading edge and high pressure towards the trailing edge, which results in rotation of the blade. At both cross-sections, the results show maximum pressure at the leading edge, due to flow stagnation caused by blade rotation. A low pressure is observed towards the windward leading edge, due to flow separation, which strengthens towards the root. A high pressure is predicted on the windward side trailing edge due to the stagnation of the incoming flow. A low pressure region is predicted on the leeward side of the blade. The negative pressure region strengthens towards the tip due to the twist of the blade, and results in vortex formation. The vortex formed on the leeward side is identified as the tip vortex.

Commented [i1]: Not labelled as (a) and (b)

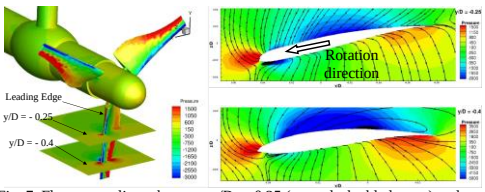

Fig. 7 Flow streamlines shown at y/D = -0.25 (towards the blade root) and y/D = -0.4 (towards the blade tip) planes to demonstrate the flow separation from the leeward side of the blade trailing edge.

URANS predicts steady flow on both coarse and medium grids, whereas IDDES predicts limited unsteadiness with <5% and < 20% resolved turbulence levels on coarse and medium grids, respectively. MILES predictions show unsteady flow with significant resolved turbulence structures, which increases with grid refinement (Fig. 8). The strut plays a significant role in triggering the resolved turbulence above the centre-plane.

The mean wake predictions shows a large streamwise velocity deficit behind the blade tips, which grows downstream, and eventually merges resulting in a peak deficit at the centerline (refer to Figs. 9a,b). The wake deficit recovery shows a sharp jump behind the strut. The velocity normal to the plane (i.e., spanwise velocity for z/D =0 plane, or transverse velocity for the y/D plane) shows positive and negative values on either side of the centerline. The velocity magnitude decays downstream but is significant up to 10% U_0 up to 7D (Figs. 9c,d). The mean cross-plane velocity, i.e., transverse velocity, for z/D = 0 plane or spanwise velocity for the y/D plane, are mostly small (< 2%U_0) (figure not shown), suggesting it does not contribute significantly to the wake diffusion towards the center.

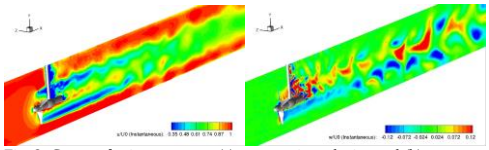

Fig. 8 Contour for instantaneous (a) stream wise velocity, and (b) transverse velocity at z/D = 0 obtained using MILES on medium grid.

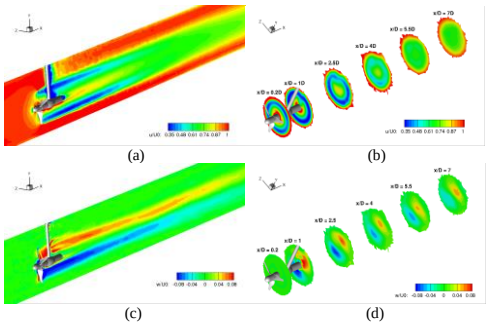

(a) (b) (c) (d)

Fig. 9 Contours for mean stream wise velocity shown at (a) z/D = 0, and (b) several x/D planes. Contours of mean transverse velocity (c) z/D = 0 and (d) x/D planes. Results are shown using MILES on medium grid.

C. Mean Wake Validation

As illustrated in Fig. 10, the experimental data shows that the peak wake deficit is higher above the center-plane than below the centre-plane. At x/D = 7, the wake deficit is just 3% for y/D = 0.5 and is about 20% for y/D = -0.5. Tedds et al. [1] attributed the asymmetry in the wake predictions, above and below the center-plane, to free-surface effects.

CFD simulations predict lower peak wake deficit above the center-plane than below the center-plane, opposite to the experimental data trends. This behavior is also evident in Fig. 9. As discussed later, the turbulence analysis suggests that the lower wake deficit above the center-plane is due to rapid shear-layer diffusion due to turbulence triggered by the struts. The wake deficit at x/D =7 is about 20% at y/D =0.5 and 34% at y/D =-0.5, significantly larger than the experimental data.

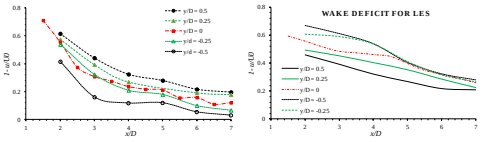

(a) (b)

Fig. 10 The peak wake deficit at different y/D locations obtained from (a) experimental data and (b) MILES on medium grid.

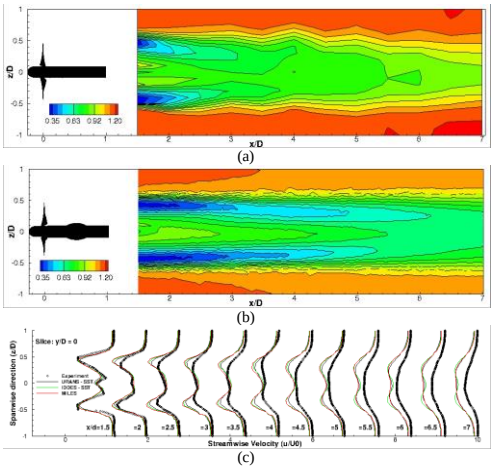

(a) (b) (c)

Fig. 11 Contour and line plots of mean stream wise velocity at y/D = 0 plane. Contour plots obtained from (a) experiment, and (b) MILES on medium grid. (c) Line plots obtained using URANS, IDDES and MILES on medium grid are compared with experimental data.

Representative plots comparing the CFD wake predictions with the experimental data are shown in Figs. 11 and 13 for the y/D = 0 plane. In the experimental data, the peak wake deficit is observed around z/D ~±0.47 at x/D =1.5, which is right behind the blade tips, and moves towards the center (Fig. 11). The wake reaches the center by x/D = 4.5. The trajectory of the peak wake defict location is shown in Fig. 12(a). As shown in Fig, 11(b), the simulations predict the high wake deficit behind the blade tip consistent with the experiment, but the deficits are much higher than the experiment. The peak deficit location is predicted well up to $x/D \leq 2.5$, but further downstream the peak wake advection towards the center is slower than the experiment. Among the simulations, MILES perfroms the best, and predicts that the wake reaches the center by x/D =8.

As shown in Fig. 11(c), the wake deficit predictions compare well with the data for $x/D \leq 2$, but show large errors

further downstream. As shown in Figs. 12(b,c), as the grid is refined, the wake deficit increases close to the turbine and the recovery rate increases in the far wake. For $x/D \leq 2$, MILES on the medium grid performes best (error E ~ 7%), followed by URANS on the medium grid (E ~ 10%); however, they both show largest errors (E ~ 30-35%) for $2< x/D \leq 5$. Further downstream, all of the simulations show similar errors (E ~ 24%). For all of the simulations, the least error is predicted for y/D = +0.5 (averaged E ~ 15%) and the maximum error (averaged E ~ 33%) for y/D = -0.25. The averaged wake prediction error in the simulations varies from 21% to 25% as shown in Table 1.

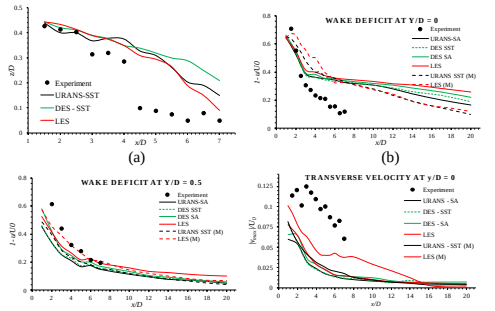

Fig. 12 URANS, IDDES and MILES predictions on coarse and medium grids are compared with experimental data for: (a) location of peak deficit at y/D = 0 plane; peak wake deficit predictions at y/D = (b) 0, and (c) 0.5 planes.; and (d) peak transverse velocity at y/D = 0.

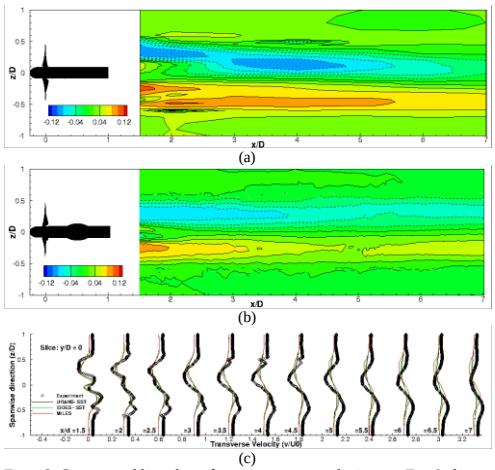

Fig. 13 Contour and line plots of mean transverse velocity at y/D = 0 plane. Contour plots obtained from (a) experiment, and (b) MILES on medium grid. (c) Line plots obtained using URANS, IDDES and MILES on medium grid are compared with experimental data.

The experimental data for the plane normal (transverse) velocity in Fig. 13 shows negative and postive values for postive and negative z/D, respectively, i.e., counter- clockwise flow, due to the swirl induced by the rotating blade. The peak velocity is about $12\%U_0$ and decreases linearly with x/D. The peak location however, shows asymmetry and the profile tends to shift towards -z/D direction. CFD predictions predict the effect of turbine blade swirl consistent with the experiment, also depicted in Fig. 9(c,d), and the results agree very well with the data in the near-wake region but show large differences further downstream. In particular, CFD predicts a faster decrease in the peak value than the experiment, and the profile is symmetric. Overall, for this velocity component, MILES results show signifacnt improvement with grid refinement and the results on the medium grid agree the best as shown in Fig. 12(d).

Experimental data for the cross-plane (spanwise) velocities show mostly intermittent postive and negative values up to x/D = 4 with peak values < $10\%U_0$. This behavior was attributed to the turbulence from the tip of the blades. CFD mean flow predictions show almost negligible cross-plane velocities–, i.e., < $2\%U_0$; however, the instantaneous flow predicts alternating positive and negative velocities due to the passage of the large-scale swirling structures.

D. Turbulent Wake Validation

Experimental data for the TKE and streamwise turbulent fluctuations are shown in Fig. 14 for the y/D = 0 plane. The data shows large TKE close to the blade tips around z/D = 0.55 for $x/D \leq 2$. The TKE peak moves slightly towards the centre and by x/D = 4.5, an almost uniform TKE is predicted in the entire blade wake region z/D = -0.45 to 0.45. The TKE peak value decreases with x/D, where the decrease is much higher close to the turbine than away from the turbine. The data also shows high TKE towards the center at x/D = 1.5, which is very rapidly dominated by the blade tip turbulence, that is not observed at x/D = 2.5. The u' profiles are very similar to the TKE profiles (Fig. 14b). A comparison of the TKE and u' data shows that only 30-40% of the TKE is contained in the streamwise component for the entire measured wake. As discussed later, [1] reported that the turbulence in the wake is primarily two-component, with w' being the other dominating term. Thus it is estimated that w' accounts for the rest 60-70% of the turbulence.

Both URANS and IDDES showed similar turbulence predictions, as for the latter resolved turbulence levels were low (Fig. 14a). All the simulations predicted significantly higher TKE values at the centre-line close to the turbine, i.e., at x/D = 1.5, due to vortex shedding from the support structure (Fig. 15). The CFD predictions in this region compares well with the experimental data. However, significant qualitative and quantitative difference are obtained elsewhere, as discussed below.

URANS/IDDES predicts the region of high TKE behind the blade tip, but the TKE values are significantly smaller than the experimental values. The TKE peak in the blade tip region increases up to x/D = 3.5 and decreases thereafter as shown in Fig. 15(a). The u' predictions compare much better with the experiment, suggesting that the primary source of error for

poor TKE prediction is errors in the w' predictions. An additional URANS-SST simulation using ν_T/ν=1 was performed to evaluate the role of inflow turbulence viscosity on the TKE prediction. Results showed that the inflow conditions do not have a significant effect on the wake predictions.

MILES fails to predict the high TKE in the blade tip wake and the turbulence starts to appear only after x/D = 4 (Figs. 14 and 15b). Thus, the prediction errors are larger than those of URANS up to x/D =4. Once the turbulence is triggered, MILES predictions are somewhat better than URANS. However, similar to URANS, u' predictions for MILES are better than TKE suggesting that the errors in the simulations are due to a failure to predict w' accurately.

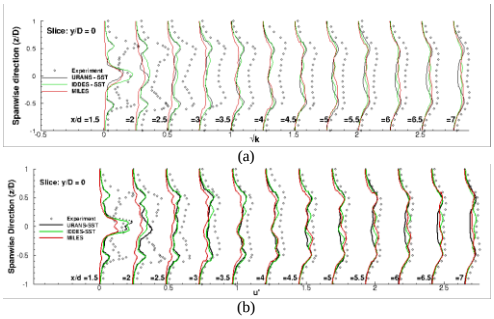

(a)

(b)

Fig. 14 (a) Streamwise turbulent velocity u' predicted by URANS-SST, IDDES and MILES on medium grid at y/D = 0 plane are compared with experimental data.

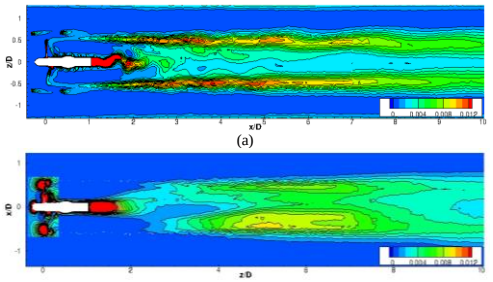

(a)

(b)

Fig. 15 TKE contour at y/D = 0 plane predicted by (a) URANS-SST and (b) MILES on medium grid. The URANS plot shows modeled component, whereas MILES shows resolved component.

The degree of turbulence anisotropy in the flow is studied using the map of the second (η) and third invariants (ξ) of the anisotropic Reynolds stresses, τ_{ij}, referred to as the Lumley triangle [39]. The stress invariants are computed as:

$$6\eta^2 = \tau_{ij}\tau_{ji} \quad (5a)$$

$$6\xi^3 = \tau_{ij}\tau_{jk}\tau_{ki} \quad (5b)$$

As shown in Fig. ~~18~~16, the origin of the invariant map, η = 0 and ξ = 0, corresponds to isotropic turbulence; the region between the η axis and 45° incline limiting line for ξ > 0 corresponds to axisymmetric turbulence with one dominant component; the region between the η axis and 45° incline limiting line for ξ < 0 corresponds to axisymmetric turbulence with two dominant components. The limiting line on the ξ > 0 side leads to 1-D turbulence when the other two turbulence components become zero. Similarly, the limiting line on the ξ < 0 side leads to axisymmetric 2-D turbulence when the third turbulence components becomes zero. The limiting line connecting the 1-D and axisymmetric 2-D turbulence marks the 2-D turbulence region.

The turbulence anisotropy in the experiment were studied in the inlet flow region, in the inner region behind the turbine ($|z/D| < 0.5$) and region outside the turbine ($|z/D| > 0.5$) for x/D = 2 – 7 for y/D = 0 data (selected plots are shown in Fig. 16). The inlet turbulence showed two dominant components - u' and w'. Invariant maps close to the turbine, at x/D = 2 and 3, shows that the turbulence is mostly single component. Since the u' contains only 30-40% of the TKE as shown Fig. 14, the dominant component is expected to be w'. Further downstream, both the inner and outer regions show mixed single- and two-component turbulence and the dominant components were identified to be u' and w'. Overall, the data showed that the turbulence gradually becomes isotropic with increasing x/D; however, even for x/D = 7, the turbulence is still strongly anisotropic.

URANS and IDDES both employed isotropic turbulence models; thus, they assume the turbulence to be isotropic. In addition, the resolved TKE level in IDDES was too small to study the turbulence anisotropy for the resolved turbulence.

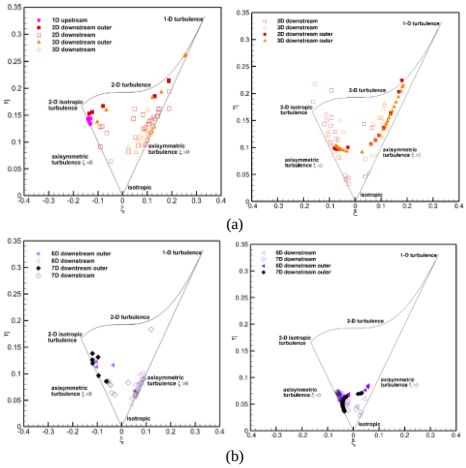

(a)

(b)

Fig. 16 Invariant maps of the Reynolds stress anisotropy tensor at (a) x/D = 2 and (b) x/D = 3 for y/D = 0 data. Inner region ($|z/D| < 0.5$) and outer region ($|z/D| > 0.5$) data are shown.

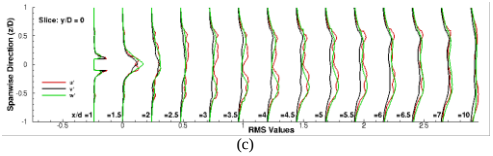

(c)

Fig. 16 Reynolds stress invariant map obtained from the experiment (LEFT panel) and MILES (RIGHT panel) (a) x/D = 2 and 2; (b) x/D = 6 and 7. (c) Comparison of streamwise, spanwise and transverse turbulent velocities predicted by MILES on medium grid at y/D = 0 plane.

The inlet turbulence is MILES is prescribed using a spectral synthesizing method wherein isotropic, random phase perturbations are generated by superimposing spectral modes with amplitudes following Kolmogrov's spectra [40]. Thus, the inlet turbulence is isotropic, in contrast to the experiment. Close to the turbine at x/D = 2 and 3, the turbulence is primarily single component dominated by w' in the outer region, whereas it is two-component dominated by u' and w' in the inner region (Fig. 16c). The CFD predictions are contradictory to the experimental data which showed one-component turbulence (dominant w') in the inner region and two-component (dominant u' and w') in the outer region. The differences are probably due to the under prediction of upstream u', along with under prediction of shear layer w'. Further downstream, the turbulence shows mixed one- and/or two-dominant components for both the inner and outer regions, consistent with the experiments. In addition, the turbulence becomes gradually isotropic with increasing x/D, also consistent with the experiment. However, the return to isotropy is faster in the CFD simulations than in the experiment.

E. Self-similarity in far wake:

The far wake profiles at y/D = 0 at x/D = 8 to 20 were analysed to evaluate the self-similarity of the wake, as shown in Fig. 17(a). The amplitude in the figure is the normalized wake deficit and the wake width is normalized by half wake width $\delta_H = 0.75U_0$. The results show very good self-similarity pattern, and compare well with a Gaussian distribution profile. Both the wake deficit amplitude and the width show a linear variation with x/D, where the former decreases with a slope of -0.016 and the latter increases with a slope of 0.031 (Fig. 17b).

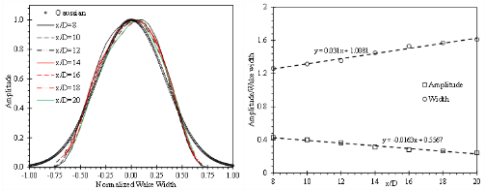

(a) (b)

Fig. 17 (a) Self-similarity in the velocity profiles compared with Gaussian curve, and (b) amplitude and wake width variation in the far-wake.

VI. CONCLUSIONS

Ansys/Fluent simulations were performed for a three-blade marine turbine appended with a support strut using URANS, DES, and LES turbulence models and resolved turbine blades on manually refined and solution adapted grids consisting of up to 8.8M cells, and the thrust, power, and mean and turbulent wake predictions for the intermediate wake ($1.5 \leq x/D \leq 7$) were compared with experimental data.

Simulations predicted unsteady thrust and power, where the largest degree of unsteadiness, approximately 8%, was predicted by LES. The simulations predicted a dominant frequency equal to the number of blades times the rotational frequency of the turbine, which is due to tower-shadow effect. The MILES also predicts an additional higher frequency due to resolved turbulence unsteadiness. The mean thrust and power coefficient predictions compared within 5% of the experimental data and did not show significant dependence on turbulence modelling.

The predictions qualitatively compared very well with the experimental data for the mean wake. Both the experiment and CFD predictions show a high wake deficit behind the blade tips, which moves towards the turbine axis; and the plane normal velocities show a counter-clockwise rotation of the flow due to the swirl induced by the rotating blade. The mean wake prediction errors were reasonably small around 7% near the blade $x/D \leq 2$, largest ~30-35% for $2 < x/D \leq 5$, and ~25% further downstream.

A synthesis of the CFD predictions and experimental data reveal that the near wake region is dominated by large-scale vortical structures generated by the turbine, which results in an annular inverted jet with inner and outer shear-layer layers. The wake recovery is primarily due to the growth of shear layers caused by the cross-plane turbulent velocity. The outer shear layer growth is primarily due to inflow turbulence while the inner shear layer growth is due to turbulence generated by the turbine. The latter is more dominant, causing the peak wake to difuse towards the center axis. In the inner region, the turbulence is primarily single-component in the near wake dominanted by cross-flow fluctuations, while it is two-component dominated by streamwise and cross-flow fluctuations in the intermediate wake, and evolves into isotropic turbulence in the far wake. The far-wake deficit shows self-similarity and follows a Gaussian profile and the wake deficit and width show linear decrease and increase, respectively, with progression.

Overall, the results show that fine grid resolution is essential for the prediction of large-scale vortical structures in the near-wake region and accurate turbulence predictions are essential for the intermediate and far wake predictions. None of the turbulence models satisfactorily predict the turbulent chracteristics of the wake, underpredicting the wake diffusion and recovery and resulting in an average 22% error for the mean wake. IDDES fails to predict the resolved turbulence satisfactorily and its predictions are similar to those of URANS. MILES performs better than others in the far-wake or above the center-plane, where the resolved turbulence is predicted. However, MILES shows the largest error in the intermediate wake as the turbulence in the blade tip region is

not predicted. The low resolved turbulence in the blade tip region is probabaly due to numerical dissipation. An ongoing simulation using a refined grid in the tip vortex region will help understand the role of numerical dissipation on MILES predictions. Future studies will focus on higher-order numerical schemes for finite-volume methods, such as those proposed by [41].

Future work will also focus on investigation between differences in CFD results and experimental data. In particular, the experimental data shows that the largest peak wake deficit occurs above the centre-plane and the lowest deficit below the centre-plane and these differences were attributed to the free-surface effects. However, CFD simulations showed the opposite trend, and the lower wake deficit above the centre-plane was due to a faster recovery caused by strut-generated turbulence. For this purpose, simulations with free-surface effects will be performed.

ACKNOWLEDGMENT

This effort was partially supported by the Center for Advanced Vehicular Systems. All simulations were performed on Talon HPC system at High Performance computing Collaboratory, Mississippi State University. The contribution of Professor Robert Poole, School of Engineering at the University of Liverpool, who provided detailed experimental data, is also gratefully acknowledged.

REFERENCES

[1] SC. Tedds, I. Owen and RJ. Poole, "Near-wake characteristics of a model horizontal axis tidal stream turbine," *Renewable Energy*, 63: 222-235, 2014.

[2] A. Kumar, T. Schei, A. Ahenkorah, R. Caceres Rodriguez, J.-M. Devernay, M. Freitas, D. Hall, A. Killingtveit, and Z. Liu, Hydropower. In IPCC Special Report on Renewable Energy Sources and Climate Change Mitigation [O. Edenhofer, R. Pichs-Madruga, Y. Sokona, K. Seyboth, P. Matschoss, S. Kadner, T. Zwickel, P. Eickemeier, G. Hansen, S. Schlömer, C. von Stechow (eds)], Cambridge University Press, Cambridge, United Kingdom and New York, NY, USA, 2011.

[3] S. Schreck, "The NREL full-scale wind tunnel experiment- Introduction to the special issue," *Wind Energy*, 5: 77-84, 2002.

[4] JN. Sørensen and W. Shen "Numerical modeling of wind turbine wakes." *J Fluids Eng;* 124:393-402, 2002.

[5] LJ. Vermeer, JN. Sørensen, and A. Crespo, "Wind turbine wake aerodynamics." *Progress in aerospace sciences*, 39(6): 467-510, 2003.

[6] RG. Elvira, A. Crespo, E. Migoya, F. Manuel, and J. Hern´andez, "Anisotropy of Turbulence in Wind Turbine Wakes". *J. Wind Eng. Ind. Aerod* , 93: 797–814, 2005.

[7] AJ. Brand, J. Peinke and J. Mann, "Turbulence and wind turbines", Journal of Physics: Conference Series, 318: 072005, 2011.

[8] G. Larsen, H. Madsen, K. Thomsen, and T. Larsen, "Wake meandering: A pragmatic approach." *Wind Energy*, 11(4):377-395, 2010.

[9] W. Shen, R. Mikkelsen, JN. Sørensen, and C. Bak. "Tip loss corrections for wind turbine computations." *Wind Energy* 8(4): 457-475, 2005.

[10] JF. Ainslie, "Calculating the field in the wake of wind turbines," J. *Wind Eng. Ind. Aerodyn*. 27: 213–224, 1988.

[11] A. Crespo, J. Hernandez, E. Frega, and C. Andreu, "Experimental validation of the UPM computer code to calculate wind turbine wakes and comparison with other models," *J. Wind Eng. Ind. Aerodyn*. 27: 77–88, 1988.

[12] P. Lissaman, "Energy effectiveness of arbitrary arrays of wind turbines," AIAA paper, 79-0114, 1979.

[13] E. Luken, and P. Vermeulen, "Development of advanced mathematical models for calculation of wind turbine wake-interaction," In: *Proceedings of EWEC'86*, Rome, 1986.

[14] M. Magnusson, AS. Smedman, "Air flow behind wind turbines," *J. Wind Eng. Ind. Aerodyn*., 80: 169–189, 1999.

[15] WZ. Shen, J. Zhang, and JN. Sørensen, "The actuator surface model: a new Navier- Stokes based model for rotor computations," *J Sol Energy Eng* , 131, 2009.

[16] I. Ammara, C. Leclerc, and C. Masson, "A viscous three-dimensional differential/actuatordisk method for the aerodynamic analysis of wind farms," *J. Solar Energy Eng.*, 124: 345–375, 2002.

[17] WMJ. Batten, ME. Harrison, and AS. Bahaj, "Accuracy of the actuator disc-RANS approach for predicting the performance and wake of tidal turbines," Phil Trans R Soc A 371: 20120293, 2013.

[18] SR. Turnock, AB. Phillips, J. Banks, and RN. .Lee, "Modelling tidal current turbine wakes using a coupled RANS-BEMT approach as a tool for analysing power capture of arrays of turbines," *Ocean Engineering*, 38: 1300-1307, 2011.

[19] T. Blackmore, W. Batten, and A. S. Bahaj, "Turbulence generation and its effect in LES approximations of tidal turbines," *Proceedings of the 10th European Wave and Tidal Energy Conference*, 2013, Aalborg, DK.

[20] N. Troldborg, JN. Sørensen, and R. Mikkelsen, "Actuator line simulation of wake of wind turbine operating in turbulent inflow," *J. Phys. Conf. Ser.* 75: 012063, 2007.

[21] MJ. Churchfield, Y. Li, and PJ. Moriarty, "A large-eddy simulation study of wake propagation and power production in an array of tidal-current turbines," *Philosophical Transactions of the Royal Society A*, 371: 20120421, 2013.

[22] J. Johansen, NN. Sørensen, JA. Michelsen, and S. Schreck, "Detached-eddy simulation of flow around the NREL phase VI blade," *Wind Energy*, 5: 185–197, 2002.

[23] A. Mason-Jones, DM. O'Doherty, CE. Morris, and T. O'Doherty, "Influence of a velocity profile & support structure on tidal stream turbine performance," *Renewable Energy*, 52: 23-30, 2013.

[24] C. Frost, CE. Morris, A. Mason-Jones, DM. O'Doherty, and T. O'Doherty, "Effects of tidal directionality on tidal turbine characteristics," *Journal of Renewable Energy*, 78: 609–620, .2015.

[25] F. Zahle, NN. Sørensen, and J. Johansen, "Wind turbine rotor–tower interaction using an incompressible overset grid method," *Wind Energy*, 12: 594–619, 2009.

[26] Y. Li, KJ. Paik, T. Xing, and PM. Carrica. "Dynamic overset CFD simulations of wind turbine aerodynamics." *Renewable Energy* 37(1): 285-298, 2012.

[27] Y. Li, AM. Castro, T. Sinokrot, W. Prescott, and PM. Carrica. "Coupled multi-body dynamics and CFD for wind turbine simulation including explicit wind turbulence." *Renewable Energy* 76: 338-361, 2015.

[28] A. Kasmi, and C. Masson, "An Extended k-ε Model For Turbulent Flow Through Horizontal Axis Wind Turbines", *Journal of Wind Engineering & Industrial Aerodynamics*, 96: 103-122, 2008.

[29] M. Shives, and C. Crawford, "Turbulence Modelling for Accurate Wake Prediction in Tidal Turbine Arrays", *5th International Conference on Ocean Energy*, Halifax, 2014.

[30] D. Cabezon, E. Migoya, and A. Crespo, "Comparison of turbulence models for the Computational fluid dynamics simulation of wind turbine wakes in the atmospheric boundary layer," *Wind Energy*, 14: 909-921, 2011.

[31] DA. Egarr, T. ~~O'doherty~~O'Doherty, S. Morris, and RG. Ayre, "Feasibility study using computational fluid dynamics for the use of a turbine for extracting energy from the tide," In *15th Australasian Fluid Mechanics Conference*, The University of Sydney, Sydney, Australia, 2004.

~~[31]~~ [31xx] A Mason-Jones, D M. O'Doherty, *C E Morris*, T O'Doherty, C B Byrne, P W Prickett, RI Grosvenor, I Owen, S Tedds, R J Poole. Non-dimensional Scaling of tidal stream turbines. *Energy*, DOI 10.1016/j.energy.2012.05.0102012, (2012)

[32] FLUENT 6.3, User Guide FLUENT 6.3. Lebanon, NH: FLUENT Inc.

[33] FR. Menter, "Two-equation eddy-viscosity turbulence models for engineering applications." AIAA journal 32(8): 1598-1605, 1994.

[34] PR. Spalart and SR. Allmaras, "A one-equation turbulence model for aerodynamic flows," La Recherche Aerospatiale 1(5), 1994.

[35] PR. Spalart, "Detached-eddy simulation." *Annual review of fluid mechanics*, 41: 181-202, 2009.

Formatted: German (Germany)

Formatted: French (France)

Formatted: German (Germany)

Formatted: Font color: Auto, Pattern: Clear

Formatted: Highlight

Formatted: Indent: Left: 0 cm, Hanging: 0.63 cm, No bullets or numbering

Formatted: Font: (Default) Times New Roman, 8 pt, Highlight

[36] AA. Adedoyin, DK. Walters, and S. Bhushan, "Evaluation of turbulence model and numerical scheme combinations for practical Finite-volume Large Eddy Simulations" *Engineering Applications of Computational Fluid Mechanics*, 9(1): 324–342, 2015.

[37] S. Bhushan, et al. "Prediction of Hydro-Kinetic Turbine Wake Characteristics using Advanced Turbulence Models," in preparation, 2016.

[38] S. Engström, H. Ganander, and L. Lindström, Short Term Power Variations in the Output of Wind Turbines, DEWI Magazine, 19, 2001.

[39] KS. Choi, and JL. Lumley, "The return to isotropy of homogeneous turbulence," *J. of Fluid Mechanics*, *436*: 59-84, 2001.

[40] R. Smirnov, S. Shi, and I. Celik. "Random Flow Generation Technique for Large Eddy Simulations and Particle-Dynamics Modeling" *Journal of Fluids Engineering*, 123:359-371, 2001.

[41] MW. Poe and DK. Walters, "A Low-Dissipation Optimization-Based Gradient Reconstruction (OGRE) Scheme for Finite Volume Simulations," *ASME-JSME-KSME 2011 Joint Fluids Engineering Conference*, Hamamatsu, Japan, 2011.

Commented [i2]: Authors in full.